Supplementary Information

A testis-specific E3 ubiquitin ligase complex governs spermiogenesis and male fertility

Tiantian Wu *et al.*

*Corresponding author: bozheng@njmu.edu.cn (B.Z.), tanyueqiu@csu.edu.cn (Y.-Q.T.), bbhxy@njmu.edu.cn (X.H.), yujun9117@126.com (J.Y.), mingxi.liu@njmu.edu.cn (M.L.)

Contents

Provided separately as Supplementary Data file

Supplementary Data 1: Proteomic profiling of ELOB-containing complexes.

Supplementary Data 2: Proteomic profiling of ASB9-containing complexes.

Source Data 1: The source data for the graphs.

Source Data 2: The uncropped blots.

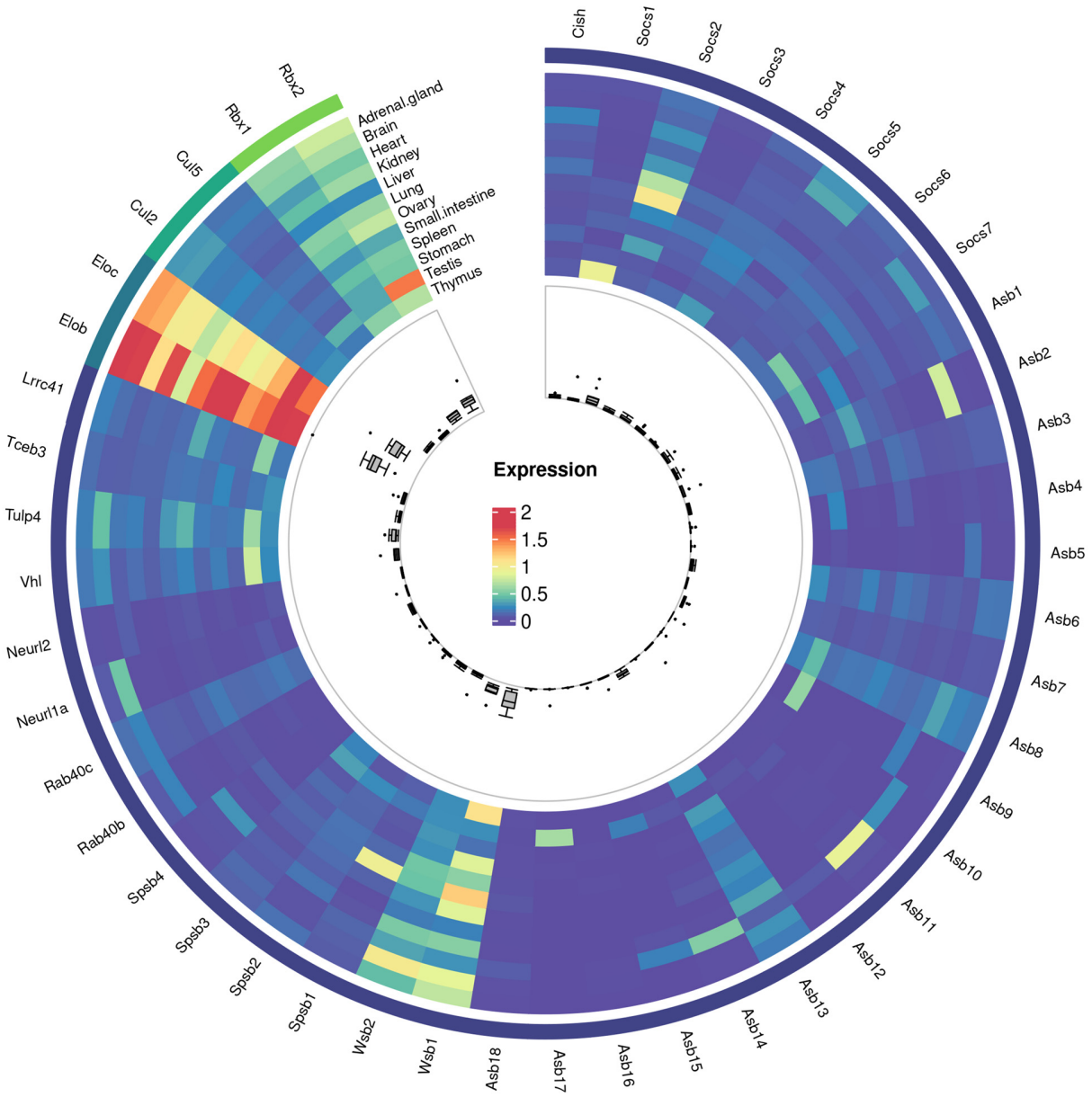

Fig. S1 Circular heatmap visualization of transcriptomic profiles for components of the ECS complex across murine tissues. Expression levels are depicted for: (i) SOCS-box-containing genes, (ii) *Elob/Eloc*, (iii) *Cul2/Cul5*, and (iv) *Rbx1/Rbx2*. Data were derived from publicly available RNA-seq datasets (NCBI SRA Project ID: PRJNA375882).

a

```
M.musculus      MDGEQRGR-----SDRPGGSPHLPFLSNPLMGDVVSDWSPLHDAAIHGCLLTLRNLISQG  55
B.taurus        -------MDGERPGRNGSKPPDMRLFSNPLMGDFVSDWSPVHEAAIHGRLLSLRSLINQG  53
M.mulatta       MDGKQGDMDGSKPAG-PRDSPDIRLLSNPLMSDAVSDWSPMHEAAIYGHQLSLRNLISQG  59
H.sapiens       MDGKQGGMDGSKPAG-PRDFPGIRLLSNPLMGDAVSDWSPMHEAAIHGHQLSLRNLISQG  59
P.troglodytes   MDGKQGGMDGSKPAG-PRDFPGIRLLSNPLMGDAVSDWSPMHEAAIHGHQLSLRNLISQG  59
                              .      * : ::*****.* ******:*:***:*  *:**.**.**

M.musculus      WPVNIITADHVSPLHEACLRGHLSCASVLLSHGAQVNGMTIDWRTPLFNACVSGSQDCVN  115
B.taurus        WPVNLITADRVSPLHEACLGGHPSCVKILLRHGANVNSVTVDWHTPLFNACVSGSHECVN  113
M.mulatta       WLVNIITADHVSPLHEACLGGHPSCVKILLKHGAQVNGVTTDWHTPLFNACVSGSRDCVN  119
H.sapiens       WAVNIITADHVSPLHEACLGGHLSCVKILLKHGAQVNGVTADWHTPLFNACVSGSWDCVN  119
P.troglodytes   WAVNIITADHVSPLHEACLGGHLSCVKILLKHGAQVNGVTADWHTPLFNACVSGSWDCVN  119
                * **:****:********* ** **.:** ***:**.:* **:********** :***

M.musculus      LLLQHGATPHPETELASPIHEAAKRGYVKCIESLAAHGANIDYNISHLGTPLYVACKNQQ  175
B.taurus        LLLQYGASPHPENDLASPIHEAAKRGHMQCIESLVAHGGDIDQNIHHLGTPLYMACENLQ  173
M.mulatta       LLLQHGASIQPESDLASPIHEAARRGHAECVDSLIAYGSNIDHKISHLGTPLYLACENQQ  179
H.sapiens       LLLQHGASVQPESDLASPIHEAARRGHVECVNSLIAYGGNIDHKISHLGTPLYLACENQQ  179
P.troglodytes   LLLQHGASVQPESDLASPIHEAARRGHVECVNSLIAYGGNIDHKISHLGTPLYLACENQQ  179
                ****:**: :**.:**********:**: :*::** *:*.:** :* *******:**:* *

M.musculus      VACAKKLLESGVSVNQGKGLDSPLHVVARMSSVELVHLLMDFGANAQAKNADGKRPVDLV  235
B.taurus        VACAKKLLESGVNVNQGRGLDSPLHAVARASSGELVSLLLDFGADTQARNAEGKRPLEVV  233
M.mulatta       RACVKKLLESGADVNQGKGQDSPLHAVARTASEELACLLMDFGADTQAKNAEGKRPVELV  239
H.sapiens       RACVKKLLESGADVNQGKGQDSPLHAVARTASEELACLLMDFGADTQAKNAEGKRPVELV  239
P.troglodytes   RACVKKLLESGADVNQGKGQDSPLHAVARTASEELAWLLMDFGADTQAKNAEGKRPVELV  239
                 **.*******..****:* *****.*** :* **.  **:****::**:**:****:::*

M.musculus      PLESPLIQIFLQNEGPQSLRQLCRLRIRKCFGIRQHHKISELLLPEDLKRFLLHL  290
B.taurus        PPESPLIQL-LQREGPSSLMQLCRLRIRKCFGIKQHHKITELNLPEELKRFLLHI  287
M.mulatta       PPDSPLARLFLEREGPPSLMQLCRLRIRKCFGIQQHHKITKLVLPEDLKQFLLHL  294
H.sapiens       PPESPLAQLFLEREGPPSLMQLCRLRIRKCFGIQQHHKITKLVLPEDLKQFLLHL  294
P.troglodytes   PPESPLAQLFLEREGPPSLMQLCRLRIRKCFGIQQHHKITKLVLPEDLKQFLLHL  294
                * :*** :: *:.*** ** **************:*****::* ***:**:****:
```

ANK SOCS box

b

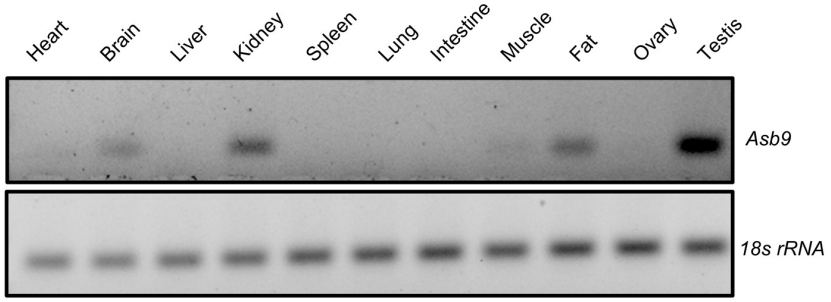

c

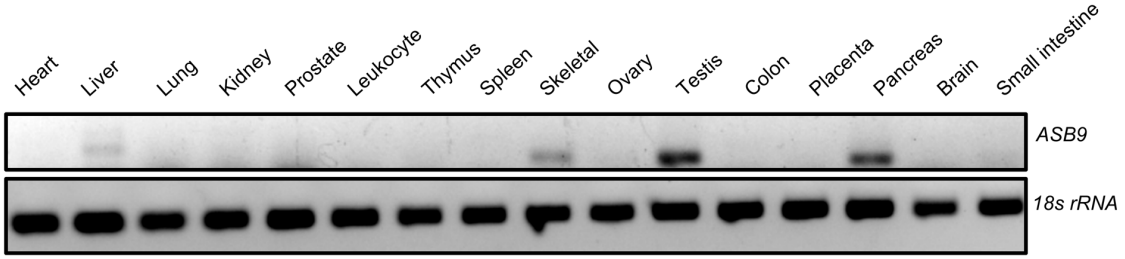

Fig. S2 Phylogenetic conservation and tissue-specific expression of the *ASB9* (*Asb9*) gene. (**a**) Amino acid sequence alignment of ASB9 orthologs across species. Domains include six ankyrin (ANK) repeats and one SOCS box (positions indicated). Sequence data sourced from UniProt (Human: Q96DX5; Mouse: Q91ZT8). (**b**) *Asb9* expression in mouse tissues analyzed by RT–PCR. (**c**) *ASB9* expression in human tissues analyzed by RT–PCR. For (b) and (c), similar results were observed from three independent experiments.

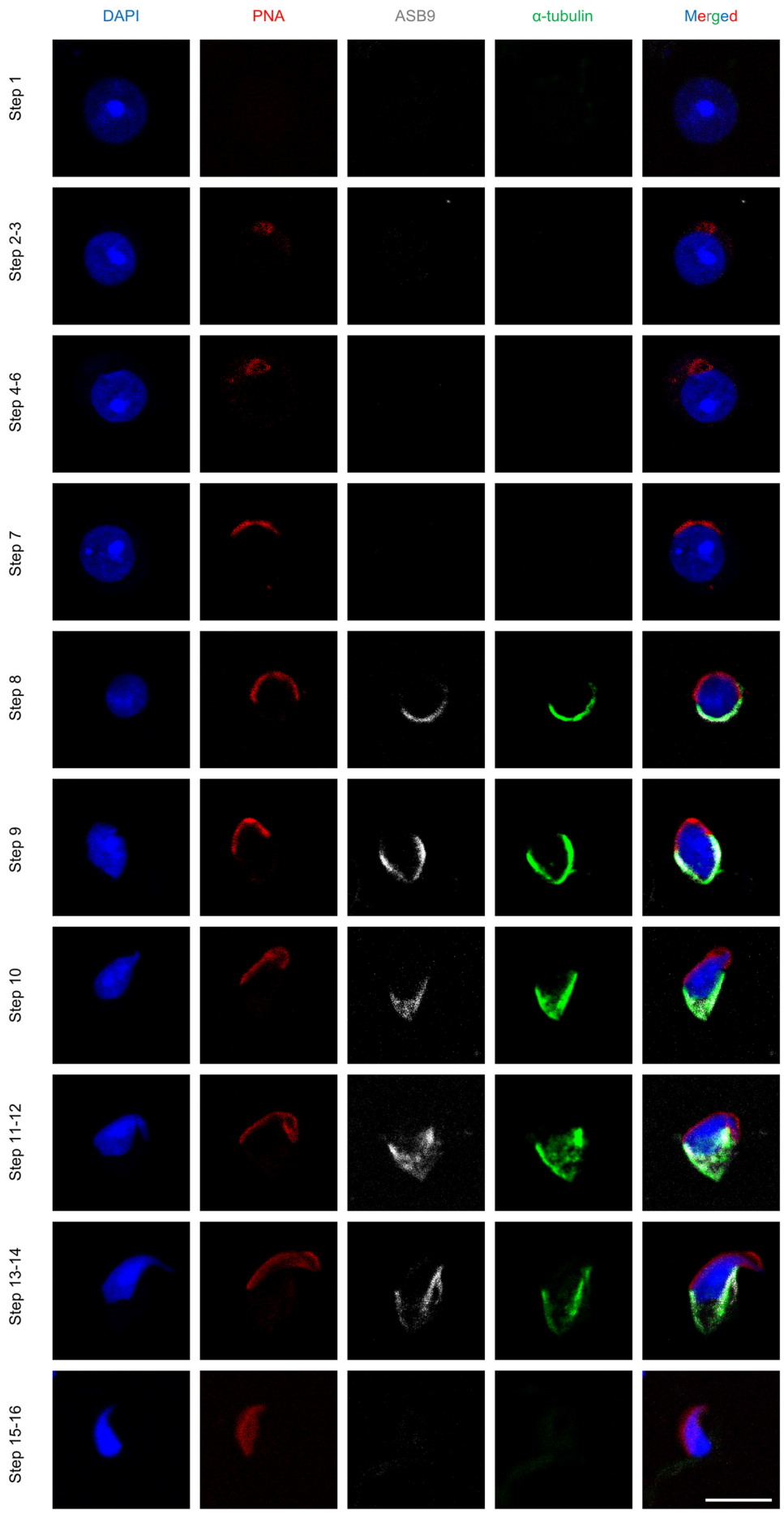
DAPI
PNA
ASB9
α-tubulin
Merged
Step 1
Step 2-3
Step 4-6
Step 7
Step 8
Step 9
Step 10
Step 11-12
Step 13-14
Step 15-16

Fig. S3 ASB9 colocalizes with α-tubulin in spermatids. Co-immunostaining of ASB9, α-tubulin, and PNA in mouse testicular single-cell suspensions. At steps 8–14 of spermiogenesis, ASB9 colocalized with α-tubulin in the manchette of spermatids. Similar results were observed from three independent experiments. Scale bar: 10 μm.

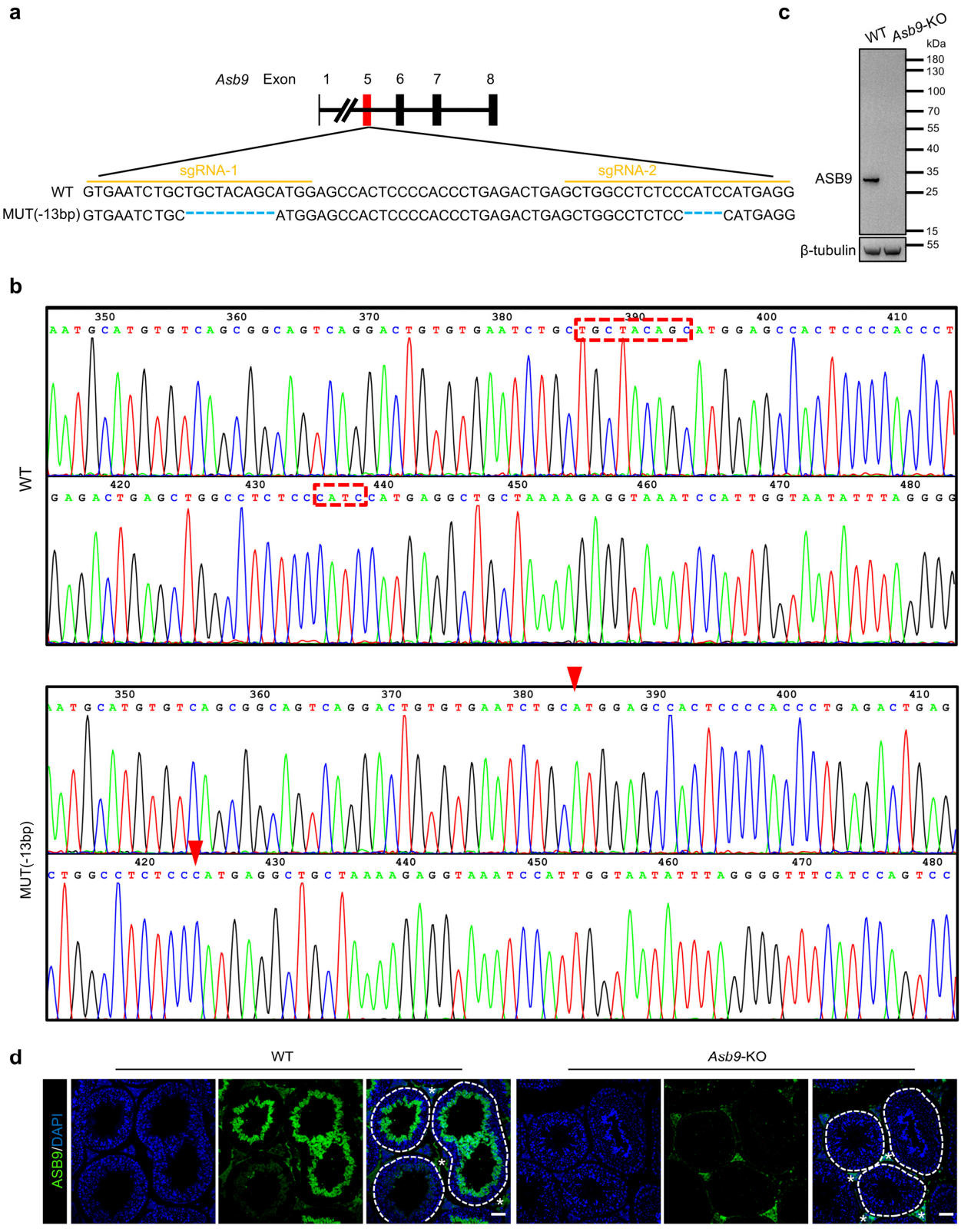
a
Asb9 Exon 1 5 6 7 8
sgRNA-1
sgRNA-2
WT GTGAATCTGCTGCTACAGCATGGAGCCACTCCCCACCCTGAGACTGAGCTGGCCTCTCCCATCCATGAGG
MUT(-13bp) GTGAATCTGC---------ATGGAGCCACTCCCCACCCTGAGACTGAGCTGGCCTCTCC----CATGAGG
c
WT Asb9-KO
kDa
180
130
100
70
55
40
35
25
15
55
ASB9
β-tubulin
b
WT
MUT(-13bp)
d
WT
Asb9-KO
ASB9/DAPI

Fig. S4 Generation and validation of *Asb9*-KO mice. (**a**) CRISPR/Cas9-mediated knockout strategy targeting exon 5 of *Asb9*. Two sgRNAs induced a 9-bp deletion in the first coding region and a 4-bp deletion in the second coding region, generating frameshift mutations. WT: wild-type; MUT: mutant. (**b**) Sanger sequencing chromatograms confirming deletions in *Asb9*-KO mice. Dashed boxes in WT traces indicate sequences absent in mutants; arrows mark mutation start sites. (**c**) Western blot analysis of testicular lysates confirming complete ASB9 protein ablation in *Asb9*-KO mice. Similar results were observed from three independent experiments. (**d**) Immunofluorescence localization of ASB9 in testicular sections. Specific spermatid signal (dashed circles) observed in WT seminiferous tubules is abolished in *Asb9*-KO mice. Asterisks denote non-specific interstitial signals present in both genotypes. Similar results were observed from three independent experiments. Scale bar: 50 μm.

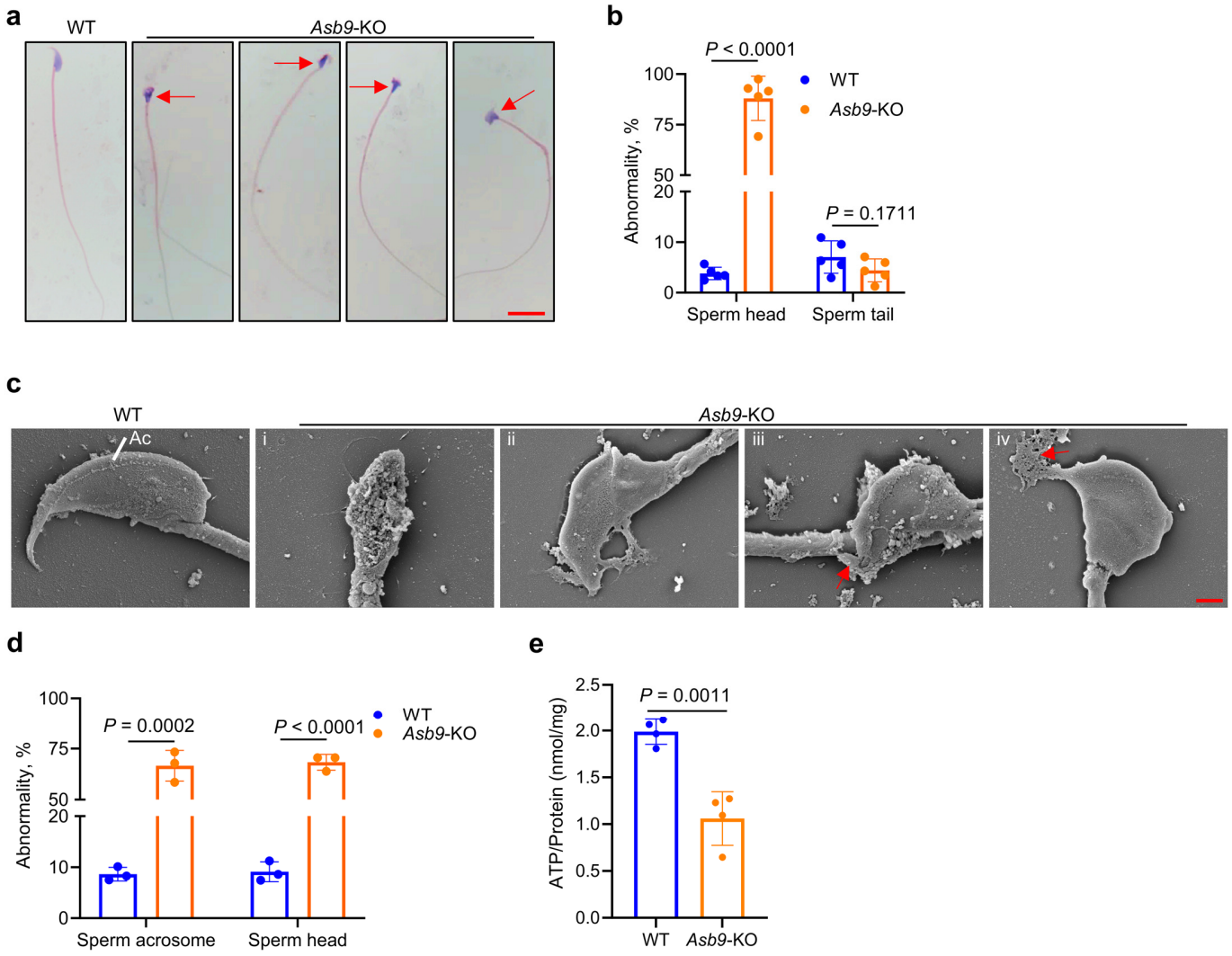

Fig. S5 Sperm head morphology defects observed in *Asb9*-KO mice. (**a**) H&E staining of caudal epididymal sperm in WT and *Asb9*-KO mice. Arrows indicate abnormal head morphologies (amorphous, small or tapered). Scale bar: 10 μm. (**b**) Quantification of (a). n = 5 mice per group. (**c**) SEM analysis showing surface topography of caudal epididymal sperm in WT and *Asb9*-KO mice. The head of WT sperm exhibits a characteristic flattened, hook-like curvature, with the acrosome, a distinct, crescent-shaped, cap-like organelle, overlying the nuclear surface. In contrast to WT sperm, *Asb9*-KO sperm exhibit misshapen and irregular heads (i-iv). Their acrosomes are severely disrupted, manifesting as either fragmentation (iii and iv; arrows) or a near-total loss (i and ii). Ac, acrosome. (**d**) Quantification of (c). n = 3 mice per group. (**e**) ATP level assay in caudal epididymal sperm of WT and *Asb9*-KO mice. n = 4 mice per group. Data are shown as means ± SD; two-sided unpaired Student's t test.

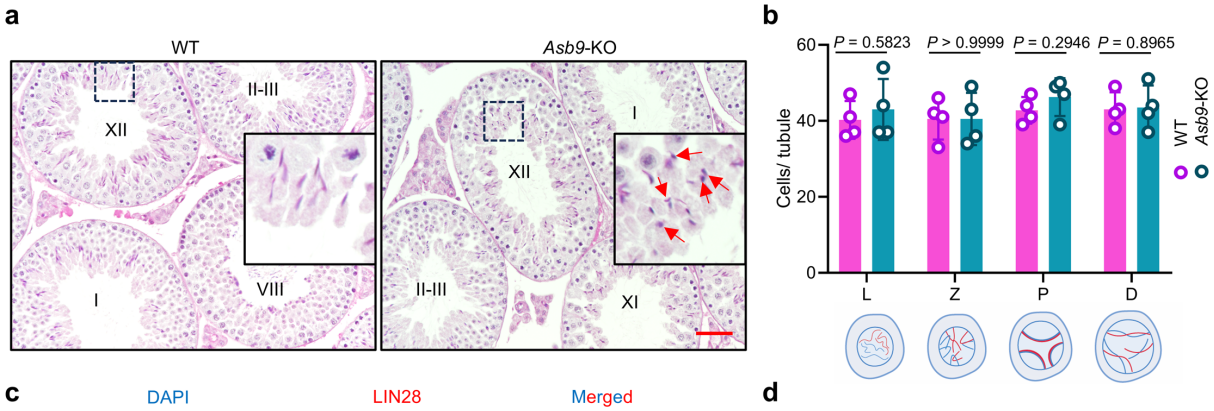
a
WT
Asb9-KO
XII
II-III
VIII
I
XII
I
II-III
XI
b
P = 0.5823
P > 0.9999
P = 0.2946
P = 0.8965
Cells/ tubule
60
40
20
0
L
Z
P
D
WT
Asb9-KO

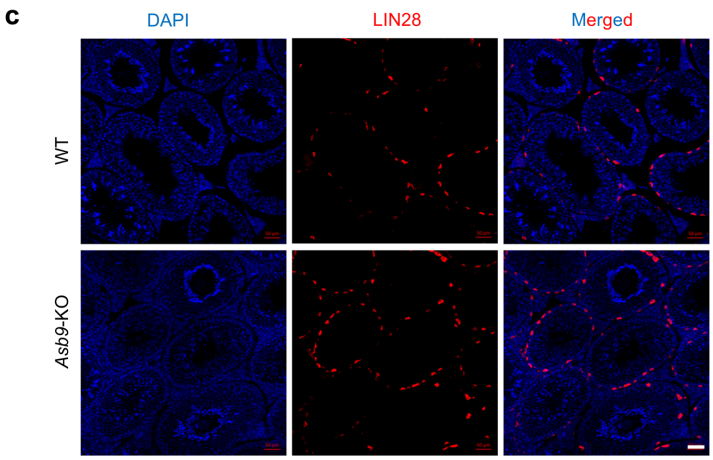
c
DAPI
LIN28
Merged
WT
Asb9-KO

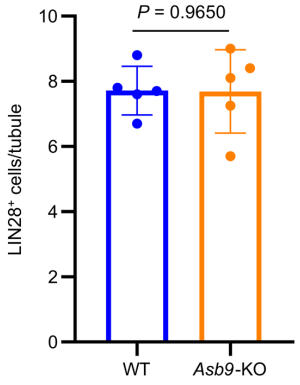
d
P = 0.9650
LIN28⁺ cells/tubule
10
8
6
4
2
0
WT
Asb9-KO

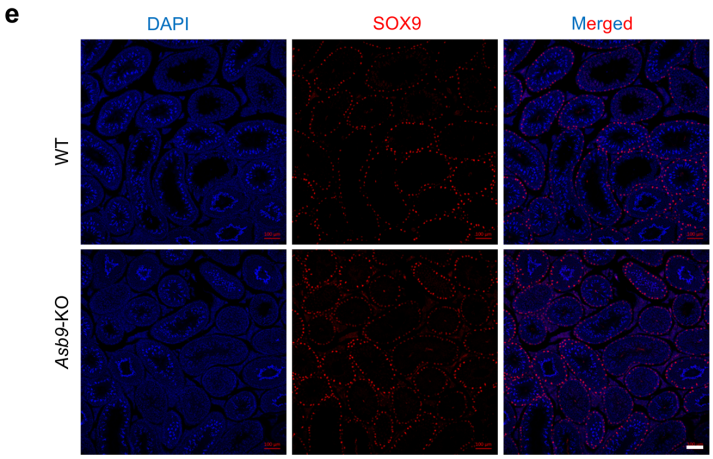
e
DAPI
SOX9
Merged
WT
Asb9-KO

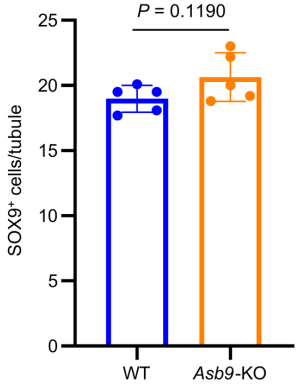
f
P = 0.1190
SOX9⁺ cells/tubule
25
20
15
10
5
0
WT
Asb9-KO

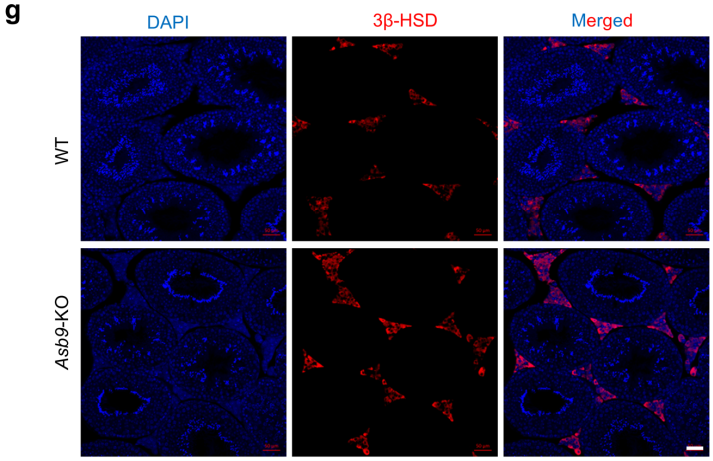
g
DAPI
3β-HSD
Merged
WT
Asb9-KO

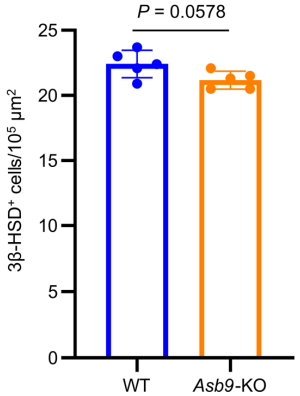
h
P = 0.0578
3β-HSD⁺ cells/10⁵ μm²
25
20
15
10
5
0
WT
Asb9-KO

Fig. S6 Histopathological and cellular characterization of *Asb9*-KO testicular defects. (**a**) PAS staining of testicular sections from WT and *Asb9*-KO mice. Red arrows indicate malformed elongating spermatids. Scale bar: 50 μm. (**b**) Quantitative analysis of meiotic prophase I spermatocytes in stage-defined tubules from (a). Leptotene (L) and pachytene (P) spermatocytes quantified in stage IX tubules; zygotene (Z) and diplotene (D) spermatocytes quantified in stage XI tubules. n = 4 mice per group. (**c**) Immunostaining of LIN28 (spermatogonia marker) in the testes of WT and *Asb9*-KO mice. Scale bar: 50 μm. (**d**) Quantification of (c). n = 5 mice per group. (**e**) Immunostaining of SOX9 (Sertoli cell marker) in the testes of WT and *Asb9*-KO mice. Scale bar: 100 μm. (**f**) Quantification of (e). n = 5 mice per group. (**g**) Immunostaining of 3β-HSD (Leydig cell marker) in the testes of WT and *Asb9*-KO mice. Scale bar: 50 μm. (**h**) Quantification of (g). n = 5 mice per group. Data are shown as means ± SD; two-sided unpaired Student's t test.

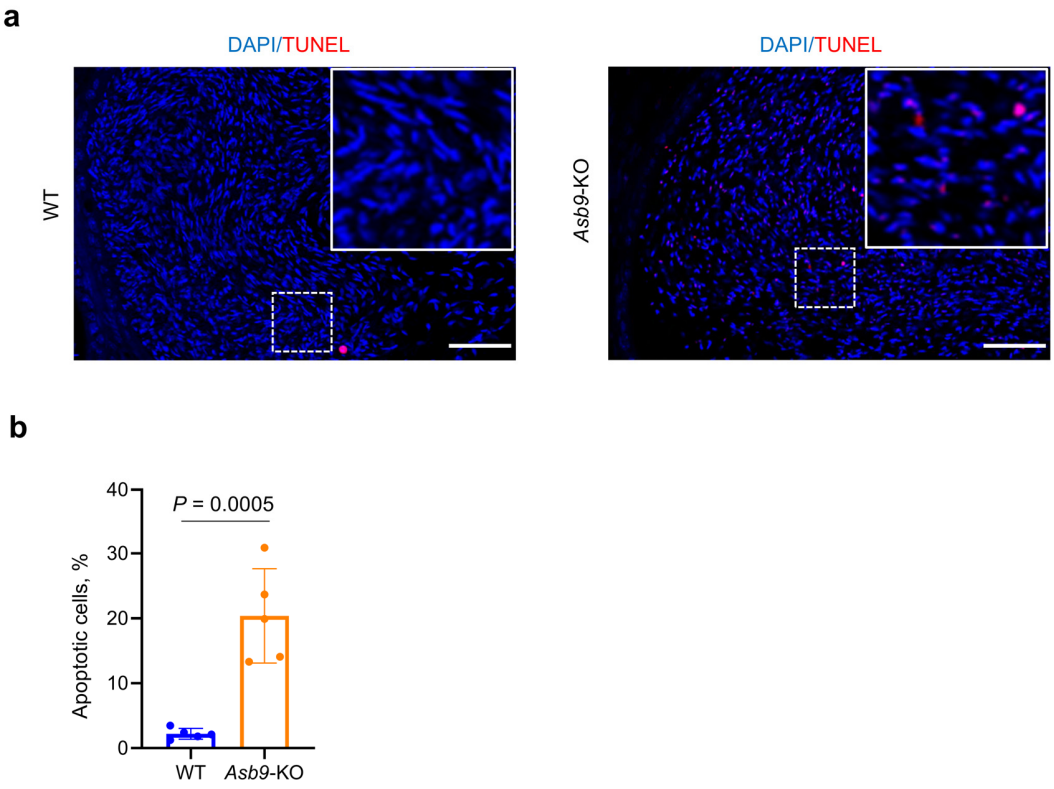

Fig. S7 Epididymal apoptosis analysis in *Asb9*-KO mice. (**a**) TUNEL assay of cauda epididymis sections from WT and *Asb9*-KO mice. Scale bar: 50 μm. (**b**) Quantification of (a). n = 5 mice per group. Data are shown as means ± SD; two-sided unpaired Student's t test.

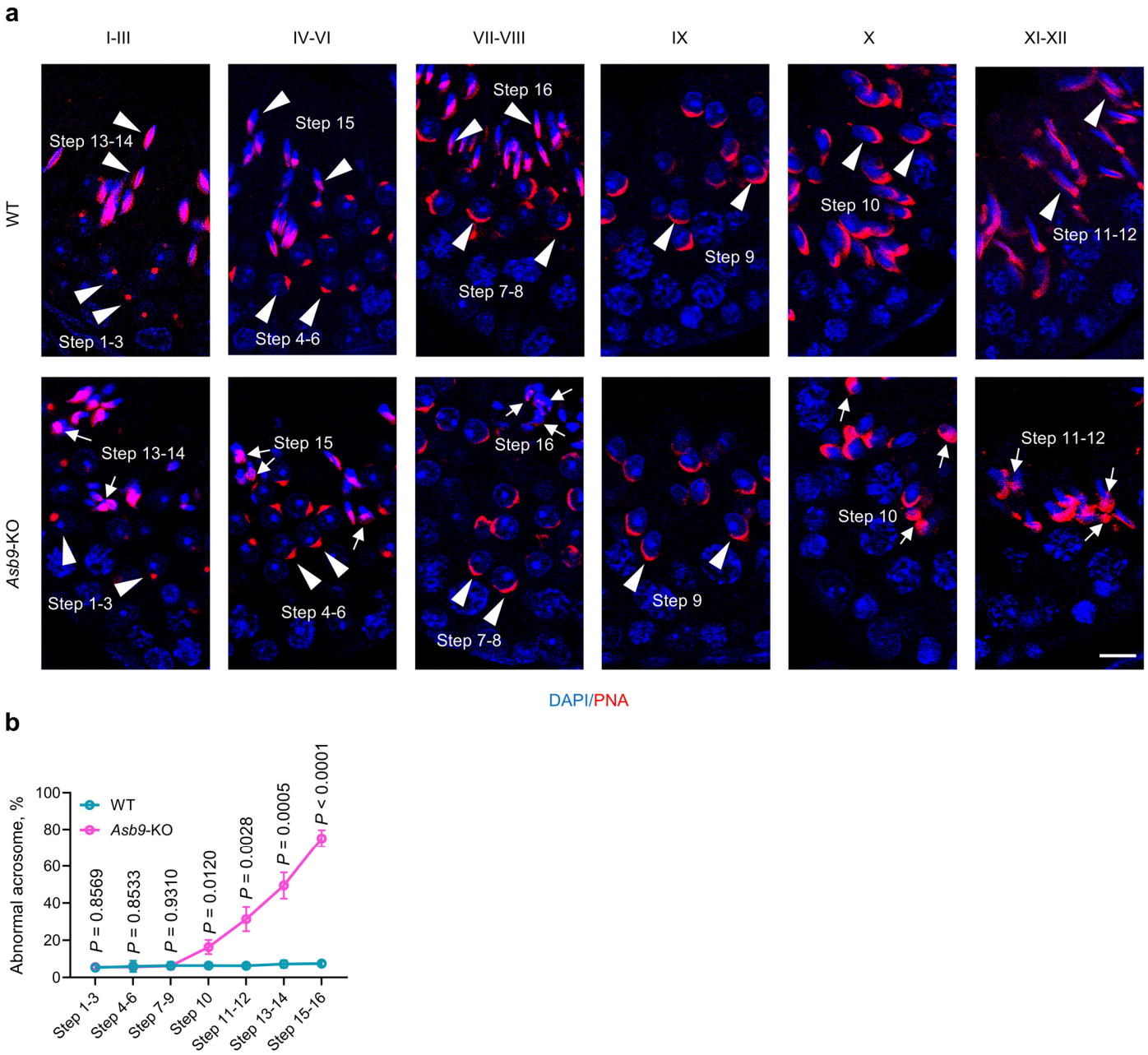

Fig. S8 Aberrant acrosome formation in *Asb9*-KO mice. (**a**) PNA staining of stages I–XII seminiferous epithelium in WT and *Asb9*-KO mice. At steps 1–9 of spermiogenesis, acrosome morphology was comparable between WT and *Asb9*-KO mice. However, from step 10 onward, when WT spermatids continued to flatten and extended to cover the nucleus, *Asb9*-KO spermatids exhibited irregularly shaped or disrupted acrosomes (arrows). Scale bar: 10 μm. (**b**) Quantification of (a). n = 3 mice per group. Data are shown as means ± SD; two-sided unpaired Student's t test.

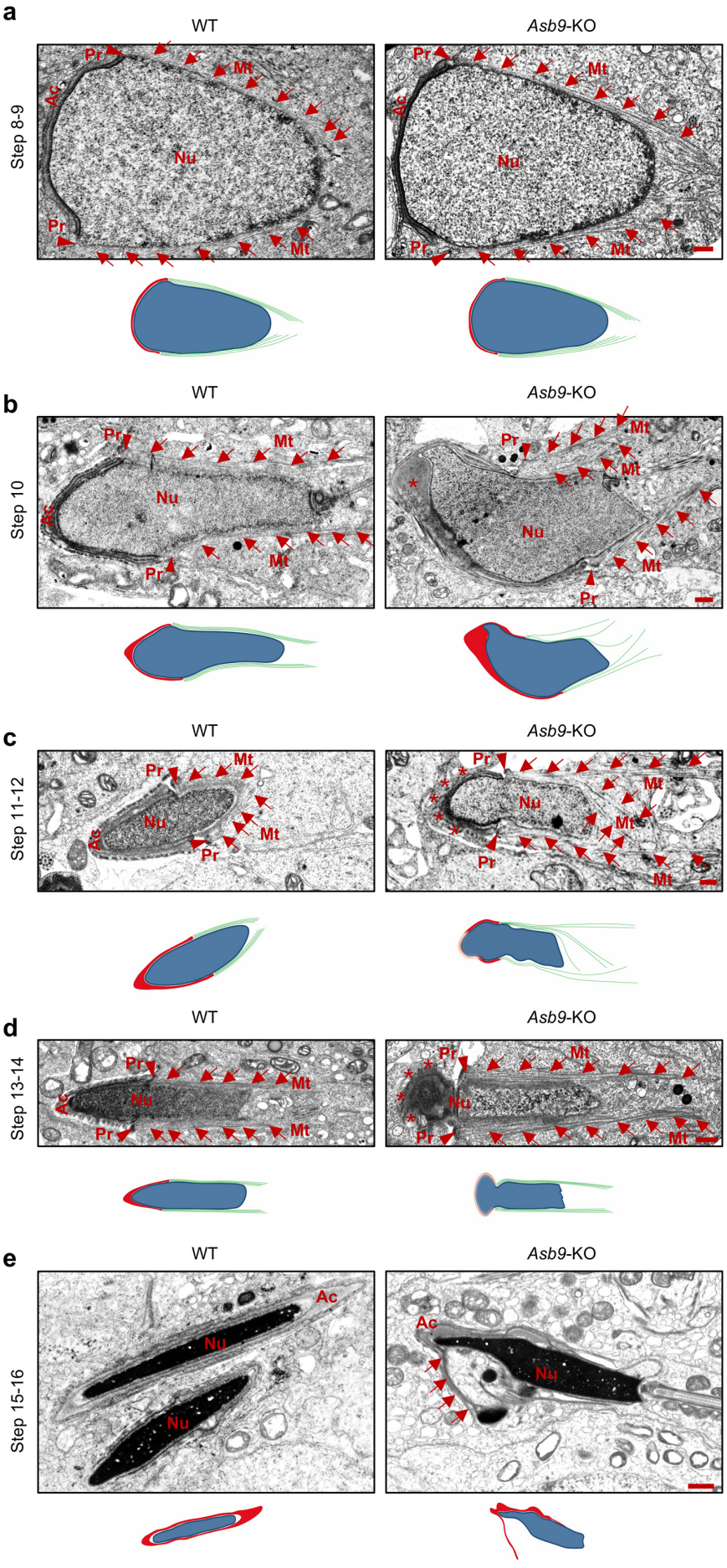
a
WT
Asb9-KO
Step 8-9
Pr
Mt
Ac
Nu
b
Step 10
c
Step 11-12
d
Step 13-14
e
Step 15-16

Fig. S9 Ultrastructural analysis of spermatid development in WT and *Asb9*-KO testes. (**a**) Transmission electron micrographs of step 8–9 spermatids. Both WT and *Asb9*-KO spermatids display characteristic bilateral flattening of the head and normally assembled manchette structures surrounding the nuclear periphery (red arrows). At this stage, the acrosome in *Asb9*-KO spermatid exhibits normal morphology and positioning, comparable to WT. (**b**) Transmission electron micrographs of step 10 spermatids. In WT spermatid, the manchette appears as a robust, organized circumferential bundle of microtubules surrounding the elongating nucleus. The nucleus exhibits normal, symmetric condensation, and the acrosome is properly positioned over the anterior nuclear surface. In contrast, *Asb9*-KO spermatid displays a thinner and less organized manchette microtubule array. Concurrently, the nucleus shows early shaping defects and asymmetrical condensation. Although the acrosome remains apposed to the nuclear envelope, it exhibits an expanded, irregular morphology (asterisk). (**c, d**) Transmission electron micrographs of step 11–14 spermatids. WT spermatids undergo further nuclear condensation and shaping, resulting in a compact head with a smoothly overlying acrosome and an appropriately sized manchette. In contrast, *Asb9*-KO spermatids exhibit severe malformations: the sperm head is misshapen, the acrosome appears irregular with a seemingly blurred boundary against adjacent structures (asterisks), and the manchette microtubules are aberrantly elongated. (**e**) Transmission electron micrographs of late spermatids/spermatozoa. In WT spermatid, removal of the manchette scaffold results in a fully remodeled, streamlined sperm head with a compact, condensed nucleus and a precisely fitted, intact acrosome covering the anterior nuclear surface. In contrast, *Asb9*-KO spermatid exhibits severe malformation, producing misshapen sperm heads with an irregular acrosome that shows areas of partial detachment (arrows). Ac, acrosome; Nu, nucleus; Mt: manchette; Pr: perinuclear ring. Scale bar: 500 nm. Similar results were observed from three mice per group.

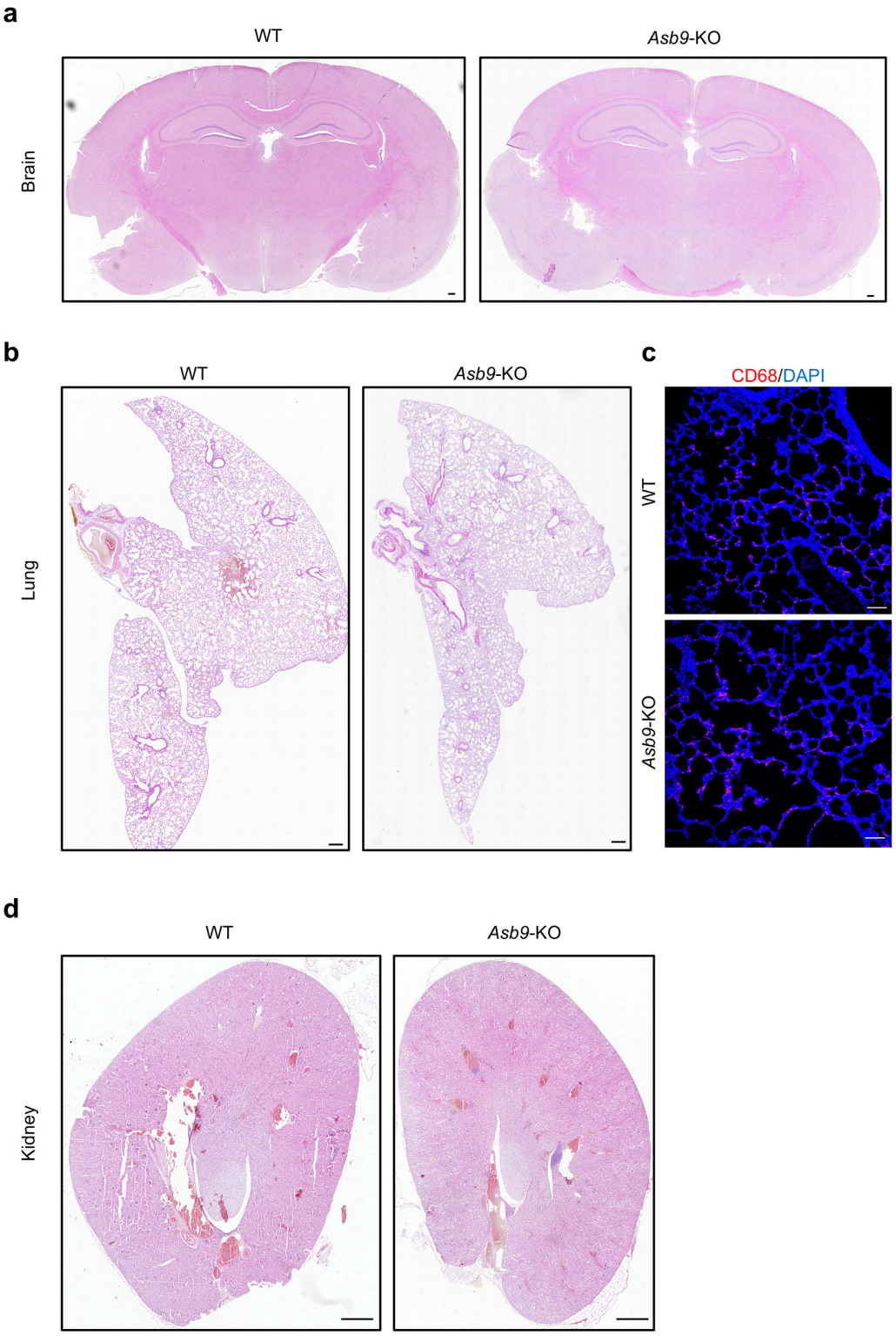

Fig. S10 Normal histology of brain, lung, and kidney in *Asb9*-KO mice. (**a**) H&E staining of brain sections in adult WT and *Asb9*-KO mice. Scale bar: 500 μm. (**b**) H&E staining of lung sections in adult WT and *Asb9*-KO mice. Scale bar: 500 μm. (**c**) Immunostaining of CD68 (macrophage marker) in lung sections of adult WT

and *Asb9*-KO mice. CD68 distribution and signal intensity were comparable between the two groups. Scale bar: 50 μm. (**d**) H&E staining of kidney sections in adult WT and *Asb9*-KO mice. Scale bar: 500 μm. Similar results were observed from three mice per group.

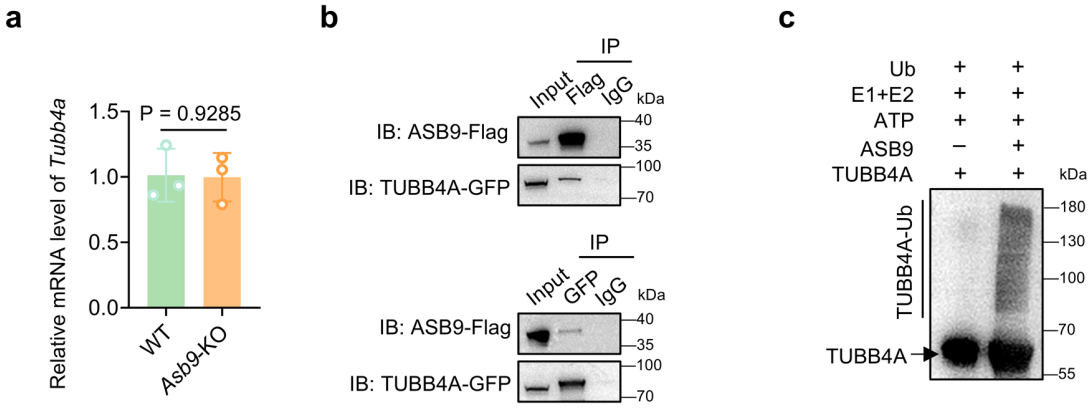

Fig. S11 ASB9 interacts with TUBB4A. (**a**) Real-time q-PCR analysis showing comparable *Tubb4a* transcript levels in 8-week-old WT and *Asb9*-KO testes. n = 3 mice per group. Data are shown as means ± SD; two-sided unpaired Student's t test. (**b**) Reciprocal co-IP assay confirming ASB9-TUBB4A interaction in HEK293T cells. Lysates from cells co-transfected with Flag-tagged ASB9 and GFP-tagged TUBB4A were immunoprecipitated with anti-Flag or anti-GFP antibodies, followed by immunoblotting with indicated antibodies. Similar results were observed from three independent experiments. (**c**) In vitro ubiquitination assay demonstrating ASB9-mediated ubiquitination of TUBB4A. Immunoprecipitated ASB9 complexes from testicular lysates (WT mice) were incubated with recombinant TUBB4A, E1, E2 (UbcH5a), ATP, and ubiquitin. Similar results were observed from three independent experiments.

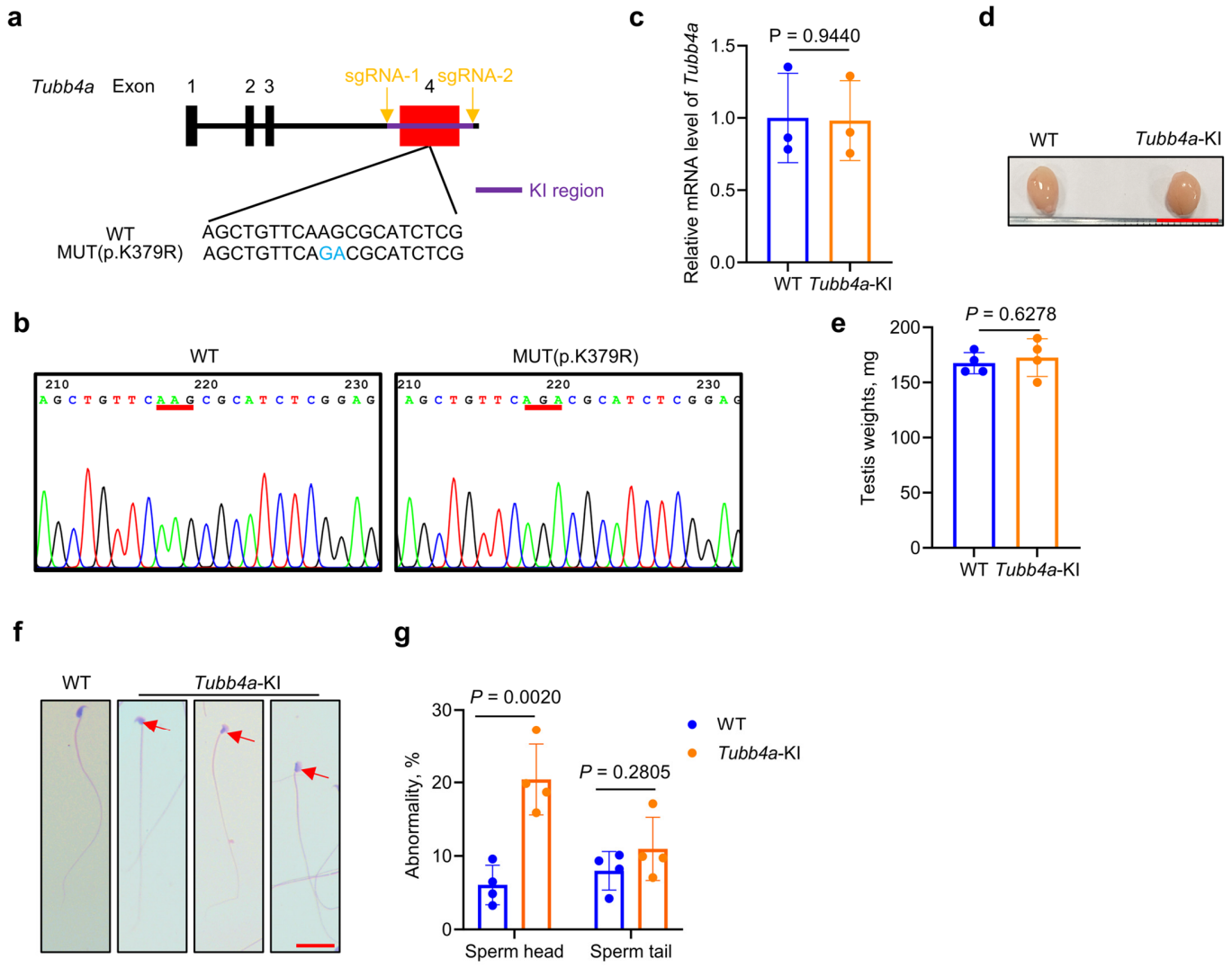

Fig. S12 Generation of *Tubb4a*-KI mice. (**a**) CRISPR/Cas9-mediated knock-in strategy for generating the *Tubb4a*$^{p.K379R}$ mutation, involving co-injection of two sgRNAs, a donor vector containing the *p.K379R* (AAG→AGA) cassette with homology arms, and Cas9 mRNA into fertilized mouse eggs to generate targeted knock-in offspring. (**b**) Sanger sequencing chromatograms confirming precise incorporation of *Tubb4a*$^{p.K379R}$ mutation. (**c**) Real-time q-PCR analysis showing comparable *Tubb4a* transcript levels in WT and *Tubb4a*-KI testes. n = 3 mice per group. (**d**) Testis size of both WT and *Tubb4a*-KI mice. Scale bar: 1 cm. (**e**) Testis weights. n = 4 mice per group. (**f**) H&E staining of sperm in the cauda epididymis of WT and *Tubb4a*-KI mice. The red arrows indicate deformed sperm heads. Scale bar: 20 μm. (**g**) Quantification of (f). n = 4 mice per group. Data are shown as means ± SD; two-sided unpaired Student's t test.

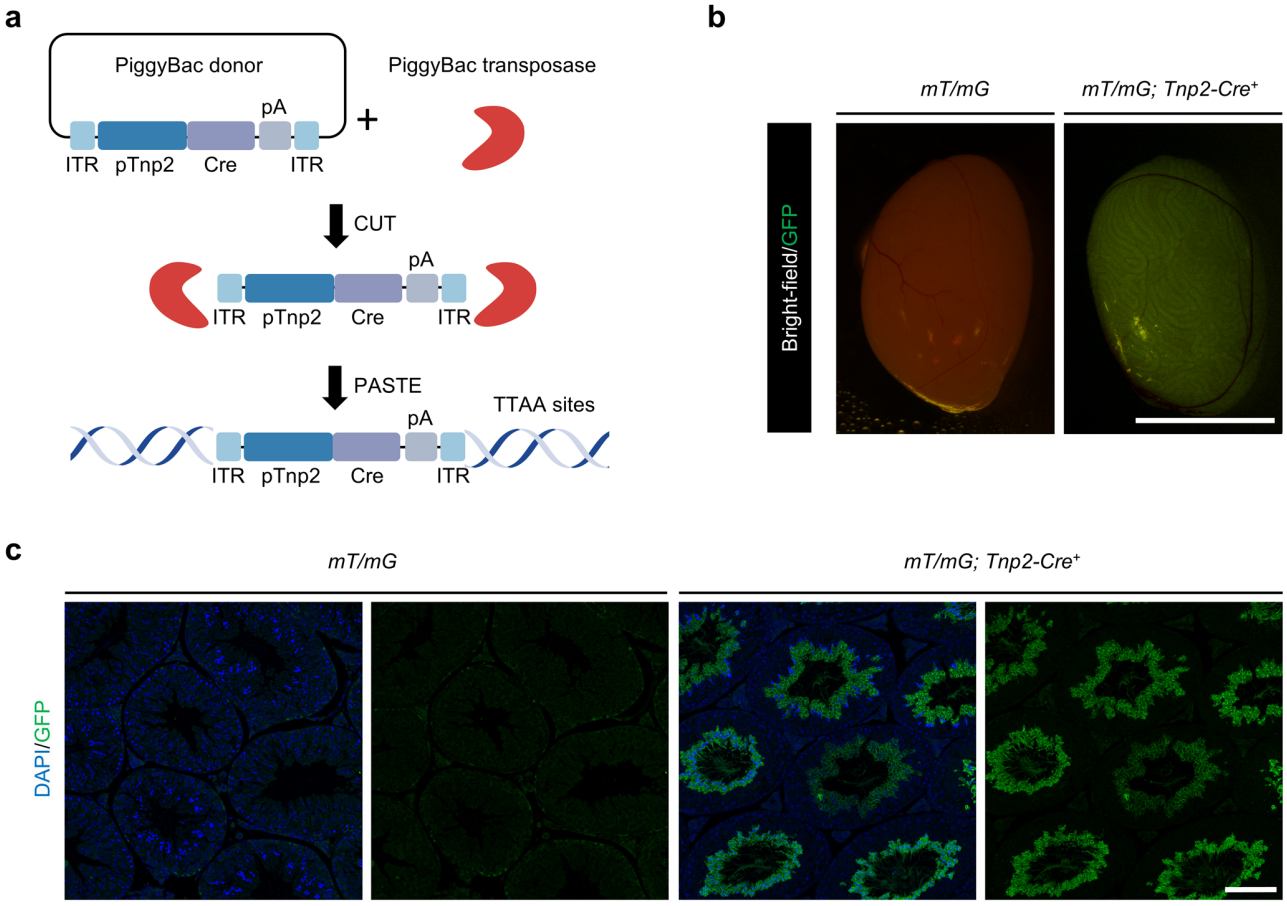

Fig. S13 Generation of *Tnp2-Cre* transgenic mice. (**a**) Schematic representation of *Tnp2-Cre* mouse generation. The donor plasmid contained the spermatid-specific *Tnp2* promoter (pTnp2), the Cre recombinase coding sequence, and a polyA tail (pA) flanked by inverted terminal repeats (ITRs). The *PiggyBac* transposase was used to cut and paste the donor sequence between the ITRs into the TTAA genomic sites. (**b**) Representative fluorescence images of the testes from *mT/mG* and *mT/mG; Tnp2-Cre*$^{+}$ mice. Endogenous GFP fluorescence indicated recombination by Cre in testes. Scale bar: 5 mm. (**c**) Immunofluorescence analysis of *mT/mG; Tnp2-Cre*$^{+}$ mouse testicular sections revealed endogenous GFP signals in the central region of seminiferous tubules. Scale bar:100 μm. Similar results were observed from three mice per group.

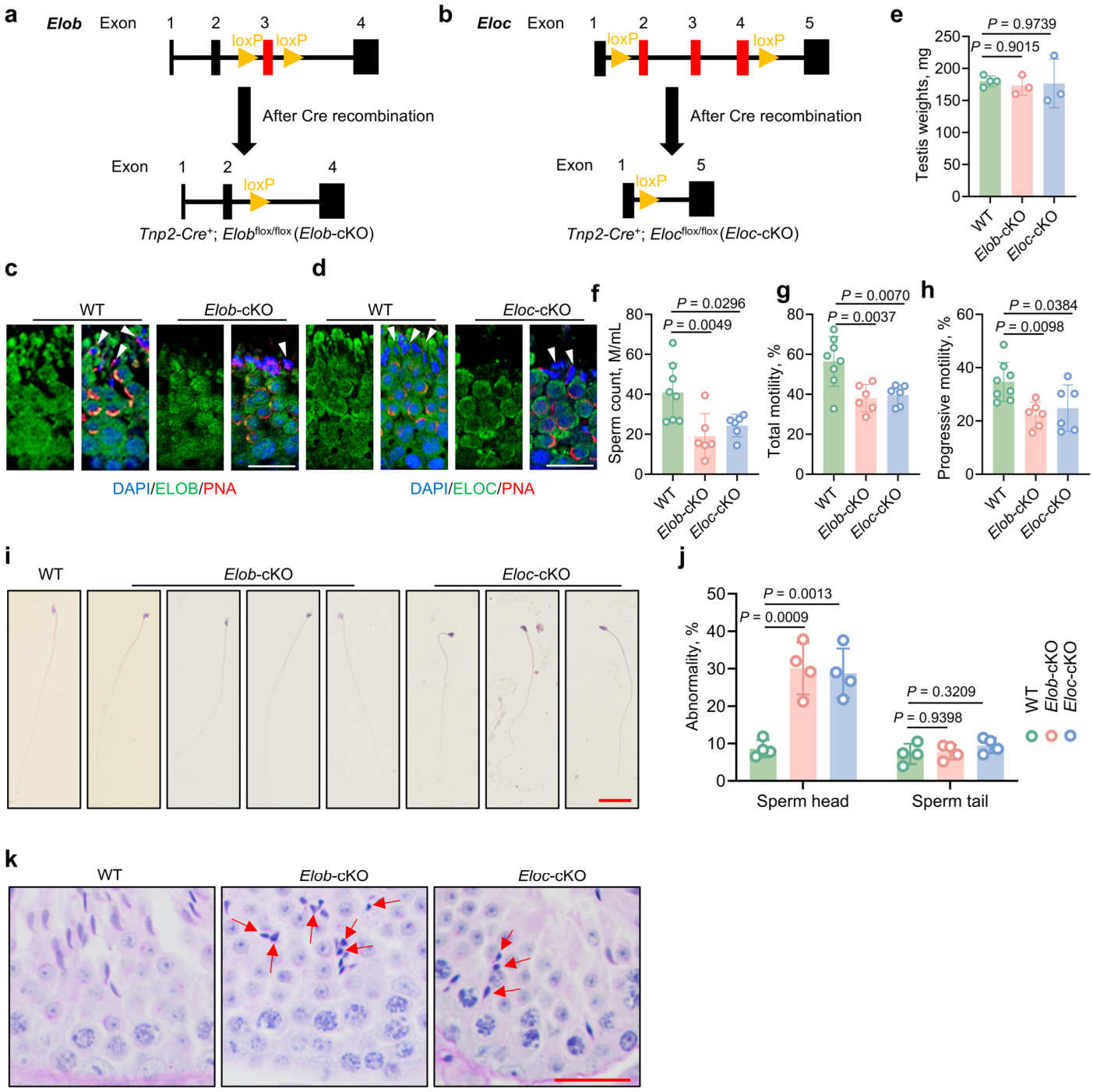

Fig. S14 Generation of *Elob/c*-cKO mice. (**a**) *Elob* cKO strategy: CRISPR/Cas9-mediated insertion of loxP sites flanking exon 3, leading to Cre-dependent excision of this exon. (**b**) *Eloc* cKO strategy: loxP sites flanking exons 2-4, enabling Cre-mediated deletion of these exons. (**c**) Immunostaining showing the absence of ELOB in elongating spermatids of *Elob*-KO mice. (**d**) Immunostaining showing the absence of ELOC in elongating spermatids of *Eloc*-KO mice. For (c and d), Similar results were observed from three independent experiments. White arrowheads: elongating spermatids. Scale bar: 20 μm. (**e**) Testis weights. n = 4 WT mice; n

= 3 *Elob/c*-cKO mice. (**f**) Sperm count from the cauda epididymis of WT, *Elob*-cKO, and *Eloc*-cKO mice. (**g**) Total motile sperm percentage measured by CASA for WT, *Elob*-cKO, and *Eloc*-cKO sperm. (**h**) Progressive motility rate measured by CASA for WT, *Elob*-cKO, and *Eloc*-cKO sperm. For (f to h), n = 8 WT mice; n = 6 *Elob/c*-cKO mice. (**i**) H&E staining showing malformed sperm heads and normal sperm tails in *Elob*-cKO and *Eloc*-cKO mice. Scale bar: 20 μm. (**j**) Quantification of (i). n = 4 mice per group. (**k**) PAS staining of testicular sections in WT, *Elob*-cKO, and *Eloc*-cKO mice. Red arrows: deformed spermatids. Scale bar: 25 μm. One-way ANOVA with Dunnett's *post hoc* test.

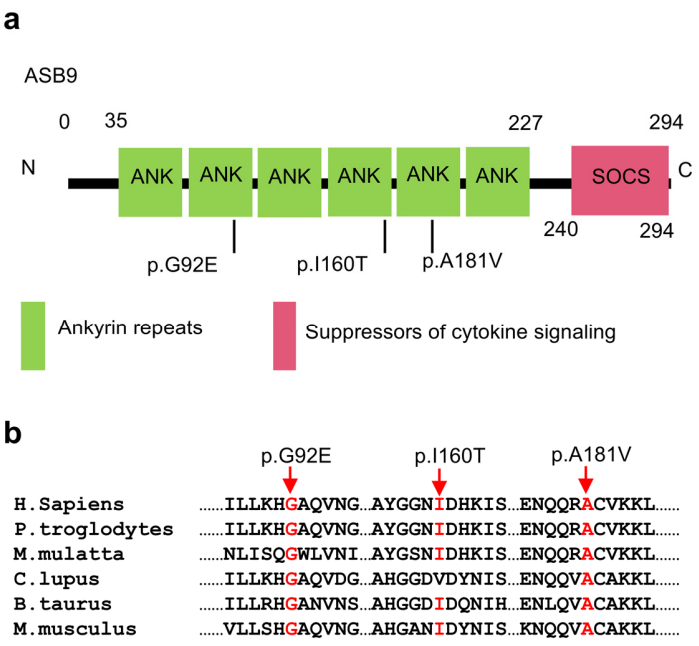

Fig. S15 Localization and evolutionary conservation of identified ASB9 mutations. (**a**) Locations of identified mutations in the ASB9 protein. (**b**) Amino acid sequence alignment of ASB9 orthologs across species. The red arrows indicate the position of *ASB9* mutations.

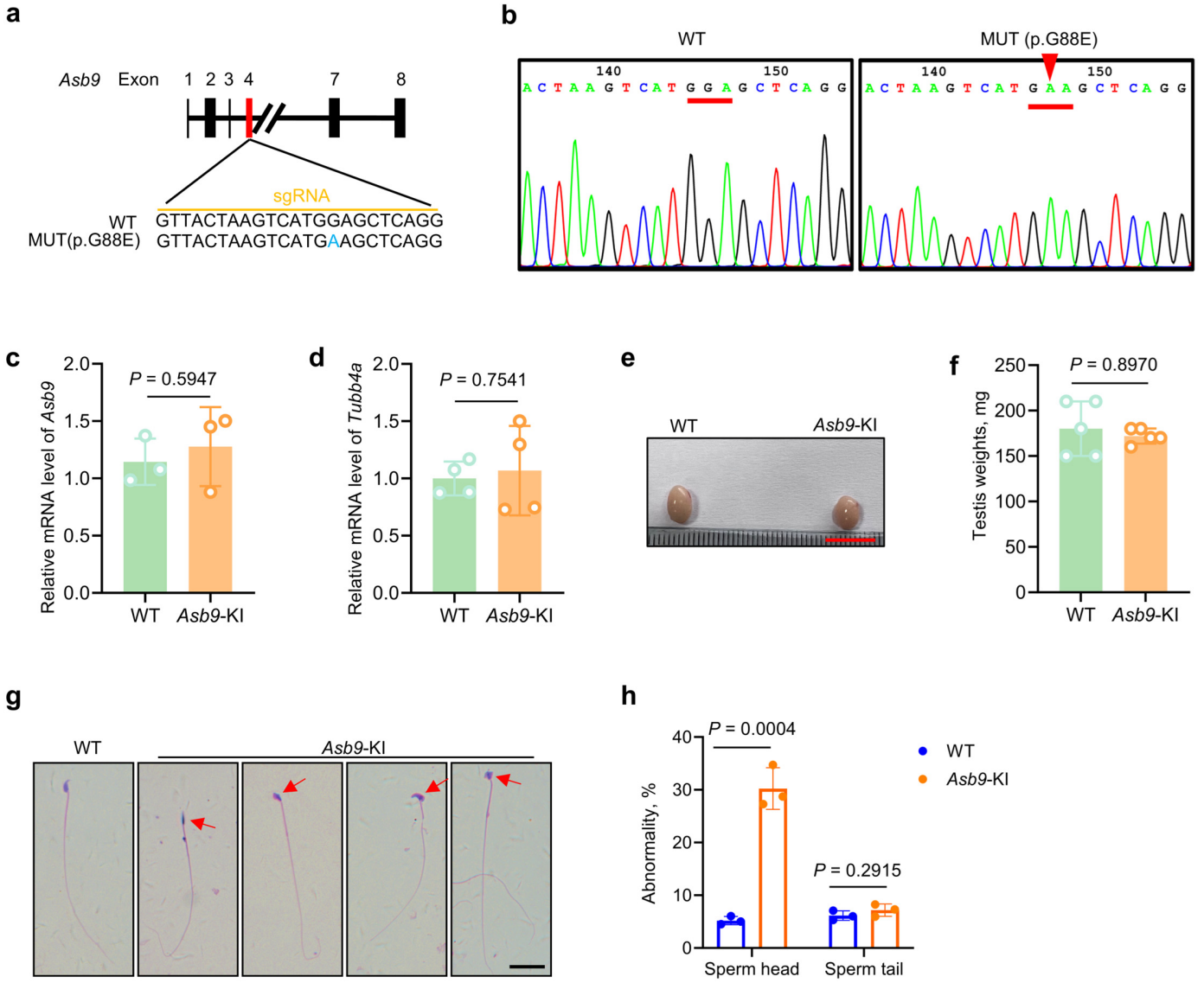

Fig. S16 Generation of *Asb9*-KI mice. (**a**) CRISPR/Cas9-mediated knock-in strategy for generating the *Asb9*$^{p.G88E}$ mutation, involving co-injection of a sgRNA, a donor oligo containing p.G88E (GGA to GAA) mutation site, and Cas9 mRNA into fertilized mouse eggs to generate targeted knock-in offspring. (**b**) Sanger sequencing chromatograms confirming precise incorporation of *Asb9*$^{p.G88E}$ mutation. (**c**) Real-time q-PCR analysis showing comparable *Asb9* transcript levels in WT and *Asb9*-KI testes. n = 3 mice per group. (**d**) Real-time q-PCR analysis showing comparable *Tubb4a* transcript levels in WT and *Asb9*-KI testes. n = 4 mice per group. (**e**) Testis size of both WT and *Asb9*-KI mice. Scale bar: 1 cm. (**f**) Testis weights. n = 5 mice per group. (**g**) H&E staining showing malformed sperm heads and normal sperm tails in *Asb9*-KI mice. Scale bar: 20 μm. (**h**) Quantification of (g). n = 3 mice per group. Data are shown as means ± SD; two-sided unpaired Student's t test.

Table S1: Novel hemizygous *ASB9* variants identified in men with oligoasthenozoospermia

***ASB9* Variant**	**M1**	**M2**	**M3**
cDNA alteration	c.542C>T	c.275G>A	c.479T>C
Variant allele	hemizygous	hemizygous	hemizygous
Protein alteration	p.A181V	p.G92E	p.I160T
Variant type	missense	missense	missense
Allele Frequency in Human Population			
1000 Genomes Project	0	0	NA
East Asians in gnomAD	0.0006	0	0
All individuals in gnomAD	0.00004568	0	1.12E-05
Function Prediction			
SIFT	damaging	damaging	damaging
PolyPhen-2	damaging	damaging	probably_damaging
CADD	22.4	26	23.5

NCBI reference sequence number of *ASB9* is NM_001031739.3

Variants with CADD values greater than 4 are considered to be deleterious.

NA, not available.

Table S2: Semen characteristics in men harboring hemizygous *ASB9* variants

Subject	**F1 II-1**	**F2 II-1**	**F3 II-1**	**F4 II-1**	**Reference Limits**
Semen Parameter					
Semen volume (mL)	5.7	2.0	3.9	3.6	1.5[a]
Sperm concentration (10^6/mL)	1.3	1.3	1.3	0.4	15.0[a]
Motility (%)	0	11.6	8.7	NA	40.0[a]
Progressive motility (%)	0	8.3	5.3	NA	32.0[a]

[a]Reference limits according to the WHO standards.

Table S3: Clinical outcomes of ICSI cycles using the spermatozoa from men harboring hemizygous *ASB9* variants

Subject	F1 II-1	F2 II-1	F3 II-1	F4 II-1
Male age (year)	41	33	39	29
Female age (year)	38	36	29	32
Number of ICSI cycles	1	1	1	2
Number of oocytes injected	10	6	6	7/8
Number (and rate) of fertilized oocytes	10(100%)	6 (100%)	6 (100%)	6(86%)/8(100%)
Number (and rate) of cleavage embryos	6 (60%)	6 (100%)	4 (67%)	6(100%)/8(100%)
Number (and rate) of 8-cells	6 (100%)	6 (100%)	4 (100%)	2(33%)/7(88%)
Number (and rate) of blastocysts	6 (100%)	6 (100%)	4 (100%)	1(50%)/7(100%)
Number of transfer cycles	1	0	1	1/1
Number of embryos transferred per cycle	2	NA	2	1/2
Implantation rate	100%	NA	50%	0%/100%
Clinical pregnancy rate	100%	NA	100%	0%/100%
Miscarriage rate	0%	NA	0%	0%/0%

Table S4: The primer sequences used in this study (5' to 3')

Gene name	Application	Sequence	Length (bp)
ASB9	Genotyping for family 1 & 3	Forward: TGGTCCCCTGGATAAGCTG Reverse: ATGAACCCTGACCTTGTCCAAC	372
	Genotyping for family 2	Forward: GCACCCCTTACTCTGACTGTT Reverse: AATCAAAAGTGCTGGAAGTTATTCA	230
	Genotyping for family 4	Forward: TTGCTTTACCTGACTCCAGAAGC Reverse: GATGGCAATGTCTTTCTAGCTAAGG	212
Asb9	Genotyping for KO	Forward: TTCTGGCTACTACTGTCTTAG Reverse: TGTGTTGGTAGGAGCATC	WT: 612; MUT: 599
	Genotyping for KI	Forward: AATGATATCAGAGGACCAACCCG Reverse: TGGCTTAAAATAGACCCCATAGACC	604
ASB9	Gene expression in mouse	Forward: ACCTTATCAGCCAGGGTTGG Reverse: TCGCCAGTCTATGGTCATGC	149
	Gene expression in human	Forward: CGGACGTGAACCAAGGGAA Reverse: AAGGGGGCCCTTCTCTC	198
Tubb4a	Genotyping for KI	Forward: TAAGAACATGATGGCTGCGTGTG Reverse: GGAGACTTAAGCCACCTCCTCTT	454
	Gene expression in mouse	Forward: TCTCGTCCAGAGCTAGAGCC Reverse: GATGACCTCCCAGAACTTGGC	144
18s rRNA	Gene expression in mouse & human	Forward: AAACGGCTACCACATCCAAG Reverse: CCTCCAATGGATCCTCGTTA	155
Elob	Genotyping	Forward: TTTTGAATAAGCTAGCCTGCGGA Reverse: AGACATGAATCCAGGCTCTAATCTG	WT: 136; Flox: 204
Eloc	Genotyping	Forward: AGTCAGTCAGCTTGTGTGTGTTA Reverse: CTCAGAACTTCAGTAGGGGCATTC	WT: 246; Flox: 319
Tnp2-Cre	Genotyping	Forward: TTACTGACCGTACACCAA Reverse: CTAATCGCCATCTTCCAG	1023

Table S5: The sgRNA target sequences in this study (5' to 3')

Name	Sequence
Asb9-KO-sgRNA-1	GTGAATCTGCTGCTACAGCATGG
Asb9-KO-sgRNA-2	GCTGGCCTCTCCCATCCATGAGG
Asb9-KI-sgRNA	GTTACTAAGTCATGGAGCTCAGG
Tubb4a-KI-sgRNA-1	CCTACAGCTGCTACCGCCTAAGT
Tubb4a-KI-sgRNA-2	CCATGTGGTGTTTCACTTACATC
Elob-cKO-sgRNA-1	CCAGAAGCGTGCCAGTAATCTAA
Elob-cKO-sgRNA-2	TGGAGCAGACTTACATGCAAAGG
Eloc-cKO-sgRNA-1	TCTGGGATGGAAGTTAAGGTGGG
Eloc-cKO-sgRNA-2	CCCAGCAGCAATTATTACATCTG

Table S6: Plasmid information

Name	Description
pcDNA3.1-NC	negative control; empty vector (EV)
pcDNA3.1-ASB9-Flag-WT	plasmid expressing Flag-labeled ASB9
pcDNA3.1-ASB9-Flag-G92E	plasmid expressing Flag-labeled ASB9, amino acid at position 92 mutated from G to E
pcDNA3.1-ASB9-Flag-I160T	plasmid expressing Flag-labeled ASB9, amino acid at position 160 mutated from I to T
pcDNA3.1-ASB9-Flag-A181V	plasmid expressing Flag-labeled ASB9, amino acid at position 181 mutated from A to V
pEGFP-N1-TUBB4A-GFP-WT	plasmid expressing GFP-labeled TUBB4A
pEGFP-N1-TUBB4A-GFP-K122R	plasmid expressing GFP-labeled TUBB4A, amino acid at position 122 mutated from K to R
pEGFP-N1-TUBB4A-GFP-K216R	plasmid expressing GFP-labeled TUBB4A, amino acid at position 216 mutated from K to R
pEGFP-N1-TUBB4A-GFP-K252R	plasmid expressing GFP-labeled TUBB4A, amino acid at position 252 mutated from K to R
pEGFP-N1-TUBB4A-GFP-K297R	plasmid expressing GFP-labeled TUBB4A, amino acid at position 297 mutated from K to R
pEGFP-N1-TUBB4A-GFP-K379R	plasmid expressing GFP-labeled TUBB4A, amino acid at position 379 mutated from K to R
pRK5-HA-Ub	plasmid expressing HA-labeled wildtype Ub
pRK5-HA-Ub-K6	other lysine mutated to arginine, only expressing lysine-6 containing HA-labeled mutant Ub
pRK5-HA-Ub-K11	other lysine mutated to arginine, only expressing lysine-11 containing HA-labeled mutant Ub
pRK5-HA-Ub-K27	other lysine mutated to arginine, only expressing lysine-27 containing HA-labeled mutant Ub
pRK5-HA-Ub-K29	other lysine mutated to arginine, only expressing lysine-29 containing HA-labeled mutant Ub
pRK5-HA-Ub-K33	other lysine mutated to arginine, only expressing lysine-33 containing HA-labeled mutant Ub
pRK5-HA-Ub-K48	other lysine mutated to arginine, only expressing lysine-48 containing HA-labeled mutant Ub
pRK5-HA-Ub-K63	other lysine mutated to arginine, only expressing lysine-63 containing HA-labeled mutant Ub
pRK5-HA-Ub-K0	all lysine mutated to arginine
pRK5-HA-Ub-K48R	plasmid expressing HA-labeled Ub, only amino acid at position 48 mutated from K to R

Table S7: The information of antibodies used in this study

Antigen	Source	Supplier	Application	Dilution	Catalogue no.
TCEB3	Rabbit	Proteintech	WB; IF	1:1000; 1:200	10502-1-AP
RBX1	Mouse	Proteintech	WB; IF	1:1000; 1:200	66716-1-Ig
ELOC	Rabbit	Proteintech	WB; IP; IF	1:1000; 10 μg/IP; 1:200	12450-1-AP
ELOB	Rabbit	Proteintech	WB; IP; IF	1:1000; 10 μg/IP; 1:200	10779-1-AP
Ub	Mouse	Santa Cruz Biotechnology	WB	1:1000	sc-8017
Ub-K48	Rabbit	Abcam	WB	1:1000	ab140601
Flag	Mouse	Sigma	WB	1:2000	F1804
GFP	Rabbit	Abcam	WB	1:1000	ab290
GFP	Chicken	Abcam	IF	1:500	ab13970
HA	Mouse	Santa Cruz Biotechnology	WB	1:1000	sc-7392
LIN28	Rabbit	Abcam	IF	1:500	ab46020
3β-HSD	Mouse	Santa Cruz Biotechnology	IF	1:200	sc-515120
SOX9	Rabbit	Millipore	IF	1:500	AB5535
TUBB4A	Mouse	Abcam	WB: IP	1:1000; 10 μg/IP	ab11315
TUBB4A	Rabbit	Abcam	WB; IF	1:1000; 1:200	ab179509
β-tubulin	Rabbit	Abcam	WB	1:5000	ab6046
α-tubulin	Mouse	Sigma	IF	1:500	T9026
CUL2	Rabbit	Abcam	WB	1:1000	ab166917
ASB9	Mouse	Santa Cruz Biotechnology	WB; IP; IF	1:1000; 10 μg/IP; 1:200	sc-166737
ASB9	Rabbit	Proteintech	IF	1:200	11952-1-AP
TOMM20	Rabbit	Abcam	IF	1:200	ab186735
Ac-tubulin	Mouse	Merck	IF	1:200	T6793